Supporting Information

High performance cathode materials for lithium-ion batteries based on phenothiazine-based covalent triazine framework

Shaoyu Lv,[a] Qimin He,[a] Ying Zhang,[a] Jingying Guo,[a] Xiangling Peng,[a] Ya Du[b] and Haishen Yang*[a]
a. Shanghai Key Laboratory of Materials Protection and Advanced Materials in Electric Power, College of Environmental and Chemical Engineering, Shanghai University of Electric Power, Shanghai 200090, China. E-mail: yanghsh@shiep.edu.cn
b. Institute of Advanced Synthesis, School of Chemistry and Molecular Engineering, Nanjing Tech University, Nanjing 211816, China. E-mail: ias_ydu@njtech.edu.cn

Reagents

Phenothiazine ($C_{12}H_9NS$, 98%), cuprous cyanide (CuCN, 99%) were purchased from Macklin, iodomethane (CH_3I, 99%), tetrahydrofuran (THF, 99%), trifluoromethanesulfonic acid (CF_3SO_3H, 99%), *N*-bromosuccinimide (NBS, 99%) were purchased from Adamas, sodium hydride (NaH, 60%) and *N*,*N*-dimethylformamide (DMF, 99.5%) were purchased from Greagent. Tetrahydrofuran was purified by distillation before use.

Characterization methods

Fourier transform infrared (FT-IR) spectra were obtained from PerkinElmer Spectrum Two FT-IR. Thermogravimetric analysis (TGA) was measured on the NETZSCH STA 409 PC/PG apparatus in a wide temperature range of 25-800 °C with a heating rate of 10 °C min^{-1} under nitrogen atmosphere. The Brunauer-Emmet-Teller (BET) specific surface area test was measured with a Micro Active for ASAP 2460 2.01 instrument. ^{13}C NMR solid-state characterization of **MPT-CTF** was performed on Bruker Avance NEO 400WB. The electronic conductivity of **MPT-CTF** and **MPT-CTF@CNT** were measured by the four-point probe resistivity tester technology. Scanning electron microscopes (SEM) was detected on JEOL JSM-7810F. Powder X-ray diffraction (PXRD) patterns were gained on Smartlab3KW. Proton nuclear magnetic resonance (^1H NMR) was acquired on a Bruker AVANCE III 400M.

Materials preparation

Synthesis of *N*-methylphenothiazine (***N*-MPTZ**).[1] Phenothiazine (5 g, 25 mmol) was dissolved in anhydrous tetrahydrofuran (THF, 125 mL) under nitrogen environment, and sodium hydride (2 g, 50 mmol) was added slowly. After stirring at room temperature for 2 h, methyl iodide (14 g, 100 mmol) was added to avoid light and stirred at room temperature. The process of the reaction was monitored by TLC. After 2 h, the reaction was completed. The organic phase was quenched with water, extracted with dichloromethane, and washed with water three times. After drying with anhydrous sodium sulfate, the organic solvent was removed by vacuum distillation to obtain a crude product. Recrystallized from petroleum ether, a white solid of 4.3 g was obtained with a yield of 90%. ^1H NMR (400 MHz, $CDCl_3$): δ 7.16 (m, 4H), 6.92 (td, J = 1.2, 7.6 Hz, 2H), 6.8 (d, J = 8 Hz, 2H), 3.37 (s, 3H).

Synthesis of 3,7-dibromo-10-methyl-10H-phenothiazine (**BMPTZ**).[2] Compound 1 (0.2 g, 0.9 mmol) was dissolved in *N,N*-dimethylformamide (DMF, 1 mL), then *N*-bromosuccinimide (NBS, 0.4 g, 2 mmol) was added, stirred in dark conditions, and heated up to 90 °C for 3 h. The process of the reaction was monitored by TLC. Then the temperature of the mixture was restored to room temperature, quenched with water, extracted with dichloromethane, and dried with anhydrous sulfuric acid, the organic solvent was removed by vacuum distillation to obtain crude product.

The white solid compound 0.3 g was obtained by column purification (200-300 mesh silica gel, petroleum ether) with a yield of 80%. ^{1}H NMR (400 MHz, $CDCl_3$): δ 7.26-7.22 (m, 4H), 6.64 (d, J = 8.8 Hz, 2H), 3.29 (s, 3H).

Synthesis of 10-methyl-10H-phenothiazine-3,7-dicarbonitrile (**MPTCN**)**.**[3] Compound 2, cuprous cyanide (CuCN, 1.3 g, 28.9 mmol) and *N,N*-dimethylformamide (DMF, 21 mL) were successively put into the schlenk bottle of 100mL, stirred and heated to 185 °C for 8 h. The process of the reaction was monitored by TLC. Then the temperature of the mixture was restored to room temperature, a 15% NaOH was added to the mixture. The mixture is filtered and washed with 15 % ammonia and deionized water. After drying, the crude product was separated by silica gel column chromatography (200-300 mesh silica gel, DCM) to obtain 1 g fluorescent yellow solid product with a yield of 70%. FT-IR Vmax / cm^{-1} : 2221 (C≡N), 1196 (C-N), 1155 (C-S), 1605, 1580, 1500, 1467 (benzene rings). ^{1}H NMR (400 MHz, $CDCl_3$): δ 7.48 (d, J = 2 Hz, 1H), 7.46 (d, J = 1.6 Hz, 1H), 7.34 (d, J = 2 Hz, 2H), 6.85 (s, 1H), 6.83 (s, 1H), 3.41 (s, 3H).

Preparation of **MPT-CTF**.[4] Compound 3 (100 mg, 0.38 mmol) and trifluoromethanesulfonic acid (CF_3SO_3H, 28 mg, 0.19 mmol) were put into the 1 × 12 cm ampoule, frozen at -78 °C, sealed with flame in vacuum, heated to 250 °C from room temperature, at a rate of 5 °C min^{-1}, and reacted for 12 h. After the ampoule was cooled to room temperature, the ampoule was opened, and the obtained solids were washed with ammonia (2 × 10 mL), ethanol (2 × 10 mL), methanol (2 × 10 mL) and dichloromethane (2 × 10 mL), and dried in vacuum at 80 °C to obtain orange-red solid (**MPT-CTF**, 80 mg). The yield is 80%. FT-IR Vmax / cm^{-1}: 1660, 1311 (triazine rings), 1605, 1580, 1500, 1467 (benzene rings), 1196 (C-N), 1155 (C-S).

Preparation of **MPT-CTF@CNT**. Compound 3 (100 mg, 0.4 mmol) and multi-walled carbon nanotubes (50 mg, 0.2 mmol, ID:5-15 nm) were put into a spherical ink tank. After adding proper amount of ethanol, the mixture was milled for 12 h, then dried and put into the 1 × 12cm ampoule with trifluoromethanesulfonic acid (CF_3SO_3H, 28 mg, 0.19 mmol), frozen at -78 °C, sealed with flame in vacuum, heated to 250 °C from room temperature, at a rate of 5 °C min^{-1}, and reacted for 12 h. After the ampoule was cooled to room temperature, the ampoule was opened, and the obtained solids were washed with ammonia (2 × 10 mL), ethanol (2 × 10 mL), methanol (2 × 10 mL) and dichloromethane (2 × 10 mL), and dried in vacuum at 80 °C to obtain gray-black solids (**MPT-CTF@CNT**, 120 mg). The yield is 80%. FT-IR Vmax / cm^{-1}: 1660, 1311 (triazine rings), 1605, 1580, 1500, 1467 (benzene rings), 1196 (C-N), 1155 (C-S).

Capacity contribution of MPT-CTF@CNT in MPT-CTF@CNT cathode electrode calculation

The composite capacity of cathode electrode of **MPT-CTF@CNT** can be regarded as the contribution of two components, as described by the following equation:

$C_{cathode}=C_{\mathbf{MPT\text{-}CTF@CNT}} + C_{conductive\ addtitives} \times R_{conductive\ addtitives} / R_{\mathbf{MPT\text{-}CTF@CNT}}$

where $C_{cathode}$, $C_{\mathbf{MPT\text{-}CTF@CNT}}$ and $C_{conductive\ addtitives}$ represent the specific capacities of the cathode electrode of **MPT-CTF@CNT**, **MPT-CTF@CNT** and conductive addtitives, respectively. $R_{\mathbf{MPT\text{-}CTF@CNT}}$ and $R_{conductive\ addtitives}$ correspond to the mass percent of the cathode electrode of **MPT-CTF@CNT**.

Electrochemical measurements

Electrochemical measurements were performed using a standard CR-2016 coin-type half-cells which consist of a working electrode, Celgard 2400 membrane, nickel foam, and stainless steel positive and negative shells. Composite active electrode (**MPT-CTF**:**CNT**=2:1) with the conductive agent (Ketjen black) and the binder

polyvinylidene fluoride (PVDF) in a ratio of 4:4:2 and a little of *N*-methylpyrrolidone (NMP) and balled into a slurry at room temperature for 2 h. The slurry was evenly coated on the dry and clean current collector aluminum foil, and dried at 80 °C for 12 h to remove the NMP solvent in the slurry. Take out the dried aluminum foil and prepare it into a circular electrode sheet with a diameter of 14 mm with a punching machine. The electrode sheet is divided and weighed, and the mass of the blank aluminum foil is subtracted to obtain the mass of the electrode material on the surface of the distributed aluminum foil, which can be multiplied by the corresponding ratio. The active material load of the pole piece is about 0.3-0.4 mg. The cells were assembled in a glove box filled with argon gas ($H_2O \leq 0.01$ ppm, $O_2 \leq 0.01$ ppm), select 1 M $LiPF_6$-EC/DMC (1:1 v/v) as the lithium battery electrolyte, and they have an equilibration time of 24 h before testing. The galvanostatic charge/discharge tests were performed in a voltage range of 1.5-4.2 V vs. Li/Li^+ on a NEWARE CT-4008 cell test instrument (Shenzhen, China). Cyclic voltammetry (CV) tests were recorded on the electrochemical workstation system (PGSTAT302N AutoLab, Metrohm, Switzerland). All the electrochemical tests were performed at room temperature.

Test method

For *ex-situ* FT-IR characterization, the batteries were disassembled in the glovebox filled with Ar, and the electrodes were washed with DMC to remove the electrolyte completely. The FT-IR signals were obtained at the states at the pristine, at the end of the initial discharge, and at the end of the 200 cycles discharge.

Supporting Figures

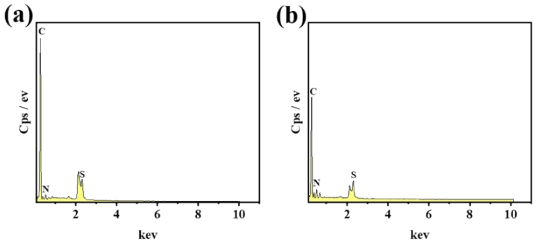

Figure S1 EDS maps of (a) **MPT-CTF@CNT** and (b) **MPT-CTF**.

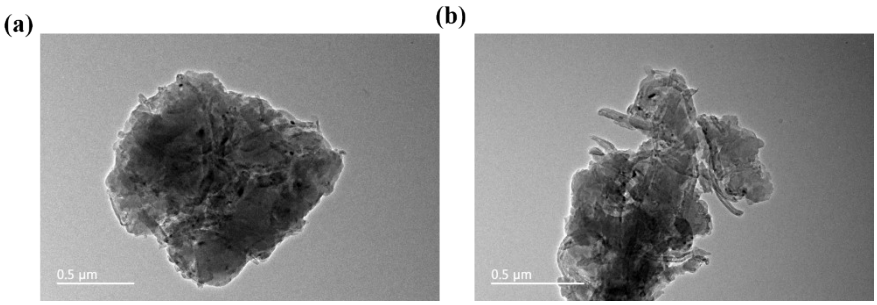

Figure S2 TEM images of **MPT-CTF@CNT**.

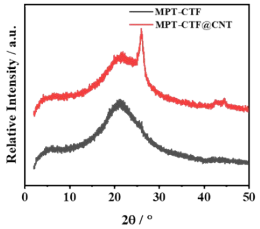

Figure S3 PXRD of **MPT-CTF** and **MPT-CTF@CNT**.

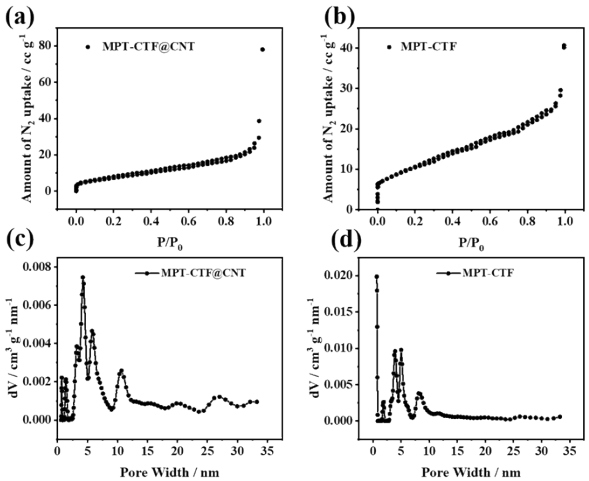

Figure S4 (a, b) N_2 adsorption isotherms of **MPT-CTF** and **MPT-CTF@CNT**; (c, d) pore size distributions of **MPT-CTF** and **MPT-CTF@CNT**.

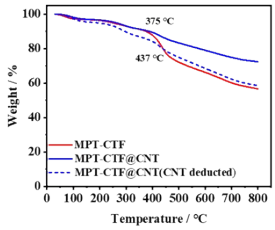

Figure S5 Thermogravimetric analysis of **MPT-CTF@CNT, MPT-CTF** under a nitrogen atmosphere with a heating rate of 10 °C min^{-1}

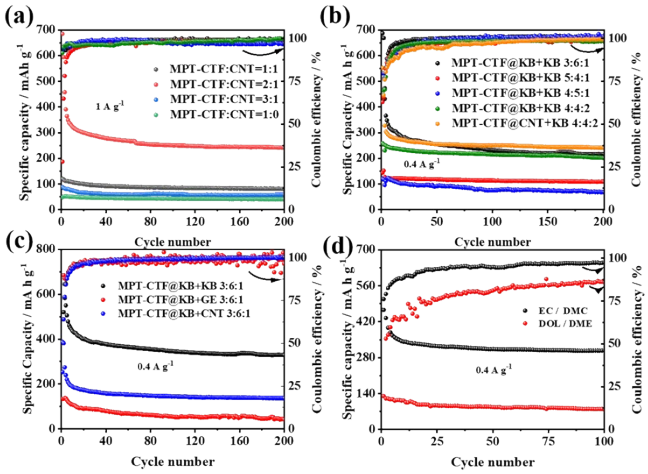

Figure S6 Electrochemical properties of (a) different composite ratios; (b) different composite materials and different cathode composite proportions (The data here is the result of deducting the contribution of conductive additive); (c) different conductive carbons; (d) different electrolytes.

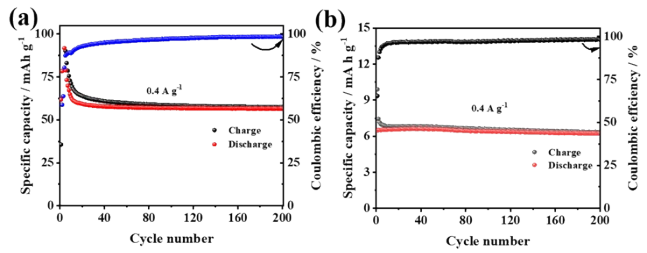

Figure S7 (a) Electrochemical property of **KB** under 0.4 A g^{-1}; (b) electrochemical property of **CNT** under 0.4 A g^{-1}.

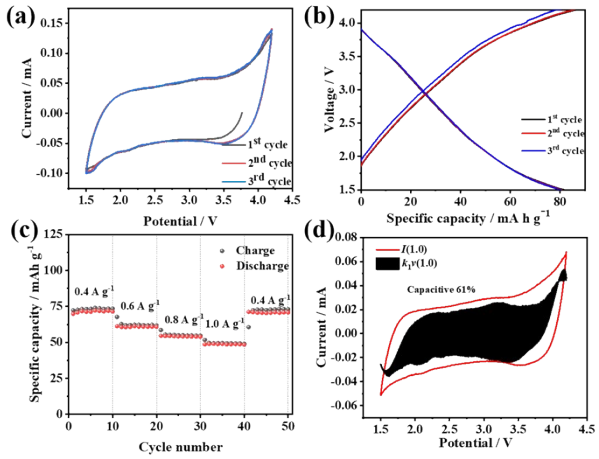

Figure S8 (a) CV curve (2mV s^{-1}); (b) charge-discharge curves of **MPT-CTF**; (c) rate capabilities at various current densities; (d) the capacitive contribution (1 mV s^{-1}) is 61% and is shown by the shaded region.

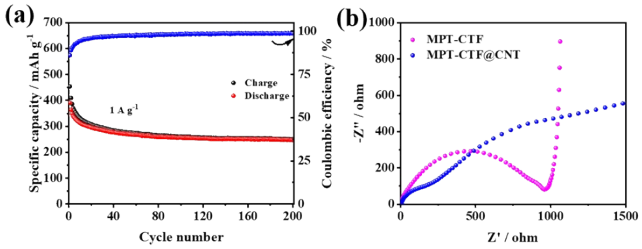

Figure S9 (a) Cycling performance of **MPT-CTF@CNT** at 1 A g^{-1}; (b) electrochemical impedance spectra (EIS) for **MPT-CTF** and **MPT-CTF@CNT**.

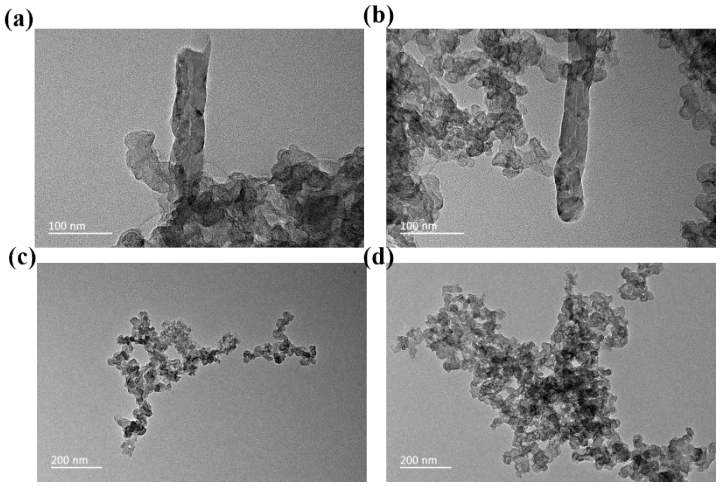

Figure S10 TEM images of (a) **MPT-CTF@CNT** electrode and (c) **MPT-CTF** electrode, (b) **MPT-CTF@CNT** electrode after 200 cycles and (d) **MPT-CTF** electrode after 200 cycles.

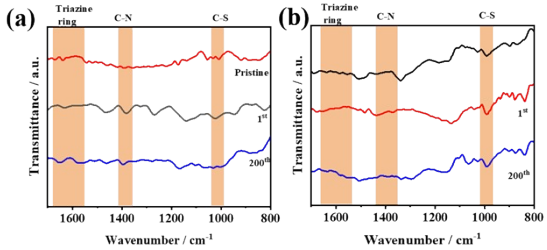

Figure S11 *Ex-situ* FT-IR spectra of (a) pristine, 1st cycle, 200th of **MPT-CTF@CNT** electrode and (b) pristine, 1st cycle, 200th of **MPT-CTF** electrode.

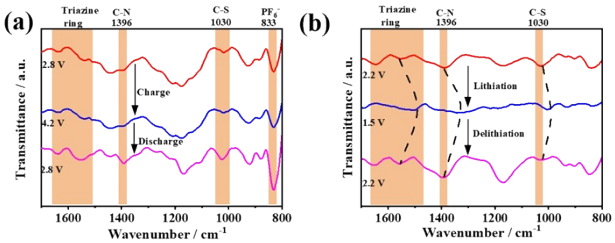

Figure S12 *Ex-situ* FT-IR spectra of the **MPT-CTF@CNT** during the charge-discharge process: (a) 2.8-4.2-2.8 V, (b) 2.2-1.5-2.2 V.

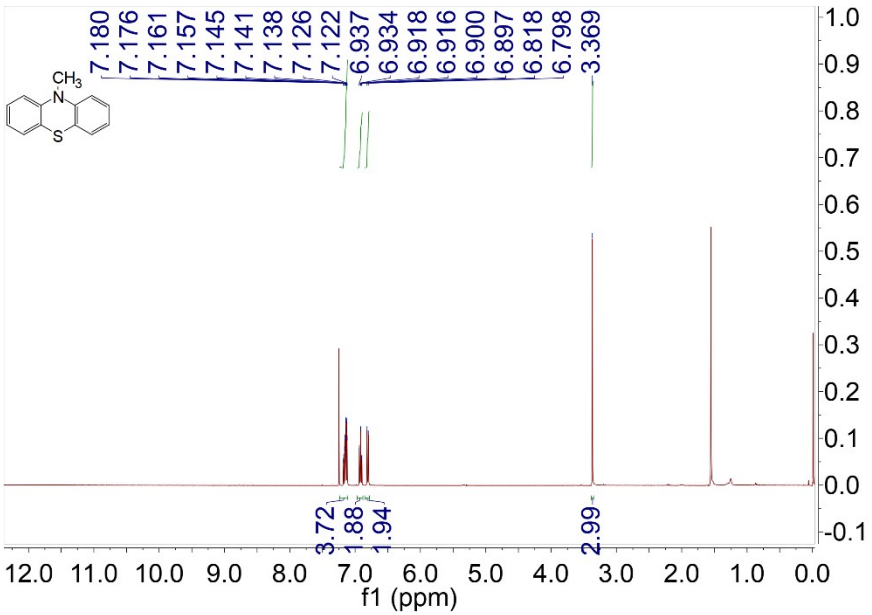

Figure S13 400 MHz ^{1}H NMR spectrum of ***N*-MPTZ** in $CDCl_3$.

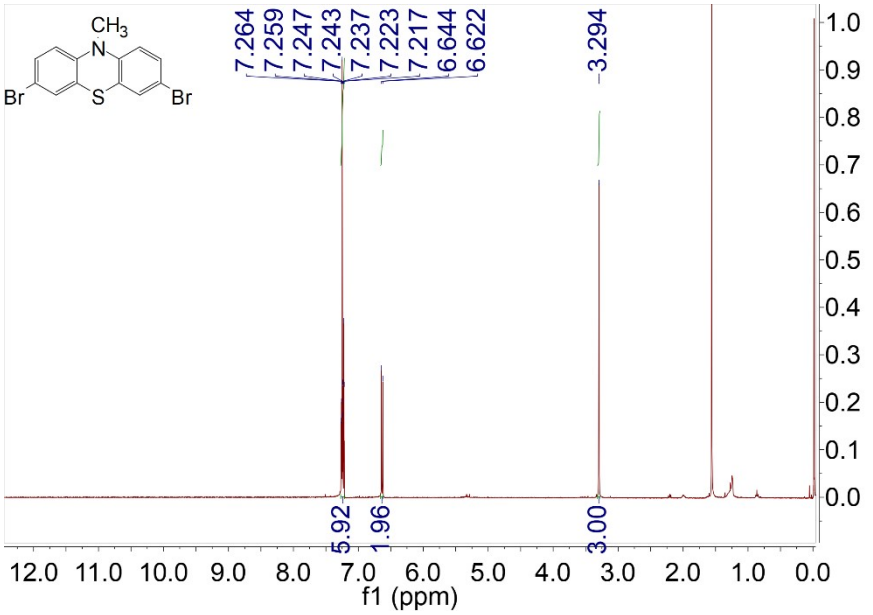

Figure S14 400 MHz ^{1}H NMR spectrum of **BMPTZ** in $CDCl_3$.

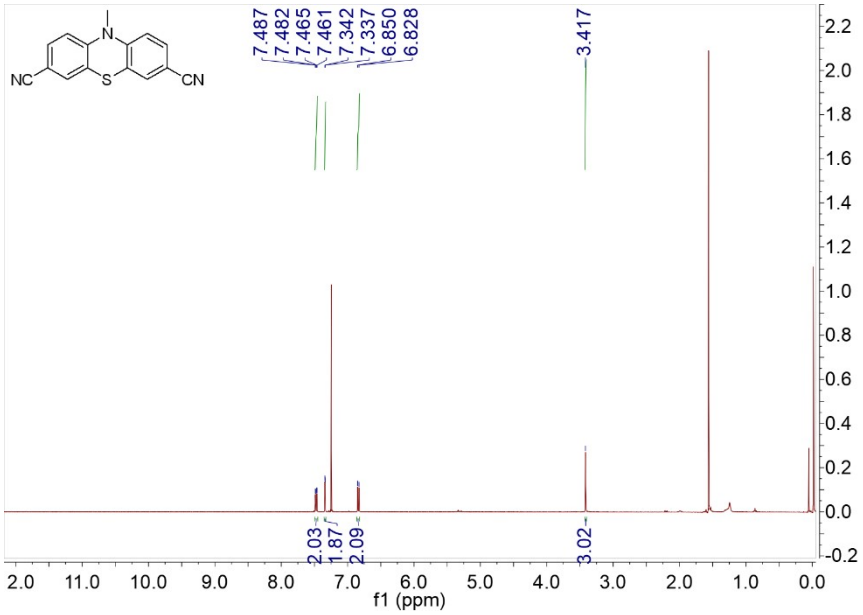

Figure S15 400 MHz ^{1}H NMR spectrum of **MPTCN** in $CDCl_3$.

Table S1 Electrical conductivity of CTFs

Covalent triazine framework	Electrical conductivity / S cm^{-1}	Ref.
IISERP-COF1_RuO2@370	2×10^{-5}	5[5]
COF-1, COF-0	1×10^{-12}	6[6]

Table S2 Electrochemical properties comparison between **MPT-CTF@CNT** in this work and previous triazine-based organic electrodes

Covalent triazine framework	Current density / A g^{-1}	Cycling number	Capacity / mA h g^{-1}	Ref.
CTF-p	0.1	50	135	7[7]
CTF-rGO	0.1	80	235	8[8]
Azo-CTF	0.1	40	205.6	9[9]
BPOE	0.01	200	40	10[10]
COF	0.057	100	102	11[11]
G-PC-800	1	500	137	12[12]
MPT-CTF@CNT	0.4/1	200/200	297/247	This work

References

1 V. K. a. L. K. R. M. Krishna, *Physical Chemistry Chemical Physics*, 1999, **1**, 2833-2939.
2 S. Pansay, N. Prachumrak, S. Jungsuttiwong, T. Keawin, T. Sudyoadsuk and V. Promarak, *Tetrahedron Letters*, 2012, **53**, 4568-4572.
3 S. Ergun, C. F. Elliott, A. P. Kaur, S. R. Parkin and S. A. Odom, *Chemical Communications*, 2014, **50**, 5339-5341.
4 Z. Yang, H. Chen, S. Wang, W. Guo, T. Wang, X. Suo, D. E. Jiang, X. Zhu, I. Popovs and S. Dai, *Journal of the American Chemical Society*, 2020, **142**, 6856-6860.
5 D. Chakraborty, S. Nandi, R. Illathvalappil, D. Mullangi, R. Maity, S. K. Singh, S. Haldar, C. P. Vinod, S. Kurungot and R. Vaidhyanathan, *ACS Omega*, 2019, **4**, 13465-13473.
6 S. Y. Li, W. H. Li, X. L. Wu, Y. Tian, J. Yue and G. Zhu, *Chemical Science*, 2019, **10**, 7695-7701.

7 Z. Wang, S. Gu, L. Cao, L. Kong, Z. Wang, N. Qin, M. Li, W. Luo, J. Chen, S. Wu, G. Liu, H. Yuan, Y. Bai, K. Zhang and Z. Lu, *ACS Applied Materials & Interfaces*, 2021, **13**, 514-521.
8 R. Yuan, W. Kang and C. Zhang, *Materials*, 2018, **11**, 937-947.
9 C. Wu, M. Hu, X. Yan, G. Shan, J. Liu and J. Yang, *Energy Storage Materials*, 2021, **36**, 347-354.
10 K. Sakaushi, E. Hosono, G. Nickerl, T. Gemming, H. Zhou, S. Kaskel and J. Eckert, *Nature Communications*, 2013, **4**, 1-7.
11 R. Sun, S. Hou, C. Luo, X. Ji, L. Wang, L. Mai and C. Wang, *Nano Letters*, 2020, **20**, 3880-3888.
12 J. Zhu, X. Zhuang, J. Yang, X. Feng and S.-i. Hirano, *Journal of Materials Chemistry A*, 2017, **5**, 16732-16739.